HHS Public Access

Author manuscript

Dev Biol. Author manuscript; available in PMC 2019 March 15.

Published in final edited form as:

Dev Biol. 2018 March 15; 435(2): 162–169. doi:10.1016/j.ydbio.2018.01.009.

The DSL ligand APX-1 is required for normal ovulation in *C. elegans*

Marie McGovern[a,b], **Perla Gisela Castaneda**[c], **Olga Pekar**[b], **Laura G. Vallier**[d], **Erin J. Cram**[c], and **E. Jane Albert Hubbard**[b,*]

[a]Department of Biological Sciences, Kingsborough Community College, City University of New York, 2001 Oriental Blvd, Brooklyn, NY 11235, United States

[b]Skirball Institute of Biomolecular Medicine, Departments of Cell Biology and Pathology, New York University School of Medicine, New York, NY 10016, United States

[c]Department of Biology, Northeastern University, Boston, MA 02115, United States

[d]Department of Biology, Hofstra University, Hempstead, NY 11549, United States

Abstract

DSL ligands activate the Notch receptor in many cellular contexts across metazoa to specify cell fate. In addition, Notch receptor activity is implicated in post-mitotic morphogenesis and neuronal function. In *C. elegans*, the DSL family ligand APX-1 is expressed in a subset of cells of the proximal gonad lineage, where it can act as a latent proliferation-promoting signal to maintain proximal germline tumors. Here we examine *apx-1* in the proximal gonad and uncover a role in the maintenance of normal ovulation. Depletion of *apx-1* causes an endomitotic oocyte (Emo) phenotype and ovulation defects. We find that *lag-2* can substitute for *apx-1* in this role, that the ovulation defect is partially suppressed by loss of *ipp-5,* and that *lin-12* depletion causes a similar phenotype. In addition, we find that the ovulation defects are often accompanied by a delay of spermathecal distal neck closure after oocyte entry. Although calcium oscillations occur in the spermatheca, calcium signals are abnormal when the distal neck does not close completely. Moreover, oocytes sometimes cannot properly transit through the spermatheca, leading to fragmentation of oocytes once the neck closes. Finally, abnormal oocytes and neck closure defects are seen occasionally when *apx-1* or *lin-12* activity is reduced in adult animals, suggesting a possible post-developmental role for APX-1 and LIN-12 signaling in ovulation.

Keywords

somatic gonad; Emo; spermatheca; reproduction; Notch; LIN-12

*Corresponding author.

INTRODUCTION

Notch signaling acts as an arbiter of cell fate during development, as a regulator of tissue stem cell fate and homeostasis, and it is implicated in a host of human diseases (see Siebel and Lendahl, 2017, for review). The *C. elegans* genome encodes two Notch receptors, LIN-12 and GLP-1. These genes have been characterized extensively for their roles in binary cell fate decisions. In embryonic development, they act, both singly and redundantly, to specify fates of blastomeres and of cells in the pharyngeal and intestinal lineages (see Priess, 2005, for review). Post-embryonically, cell fate transformations occur in a wide variety of cell types upon loss of *lin-12*, and premature differentiation of the germ line occurs upon loss of *glp-1* (see Greenwald, 2013, for review). The *C. elegans* genome encodes 10 “Delta Serrate LAG-2” (DSL) family ligands (Chen and Greenwald, 2004), LAG-2, APX-1, ARG-1, and DSL-1 to DSL-7, a subset of which have been linked to specific aspects of LIN-12 and/or GLP-1 signaling (Greenwald, 2013).

While Notch signaling is best characterized for cell fate specification during development, Notch signaling also regulates post-developmental processes including cellular reprogramming, morphogenesis, and neuronal guidance and function. In *C. elegans*, post-embryonic reprogramming from an epithelial to a neuronal cell is under the control of LIN-12/Notch signaling (Jarriault et al., 2008), as is the regulation of vulval precursor cell plasticity during diapause states (Karp and Greenwald, 2013). Morphogenesis roles include tubular morphogenesis (Rasmussen et al., 2008), vulval epithelia (Sundaram and Greenwald, 1993), vulval muscles (Li et al., 2013), and neurite morphology that impacts thermotaxis (Wittenburg et al., 2000). Post-mitotic neuronal function is also modulated by Notch signaling in the contexts of locomotion (Chao et al., 2005), chemosensory response and molting quiescence (Singh et al., 2011), as well as the decision to enter and exit the dauer diapause state (Ouellet et al., 2008). Finally, adult germline cytoplasmic flow and oocyte growth are regulated by GLP-1 (Nadarajan et al., 2009).

In the presence of sperm, *C. elegans* adult hermaphrodites produce oocytes continuously. Oocytes line up in the oviduct and undergo maturation, ovulation and fertilization in an assembly-line fashion. The proximal-most oocyte undergoes meiotic maturation in response to hormonal stimulation by the major sperm protein (MSP); this maturation is coordinated with changes in oocyte morphology and regulation of somatic gonadal sheath contractions and spermathecal dilation that together allow the maturing oocyte to be smoothly ovulated into spermatheca, where it is fertilized. The zygote then passes through the spermathecal-uterine valve into the uterus (see Kim et al., 2013, for review). Oocytes that undergo meiotic maturation while being retained in the oviduct undergo endoreduplication, leading to an EndoMitotic Oocyte (Emo) phenotype, characterized by polyploid oocyte nuclei easily visible with DNA dyes such as DAPI (Iwasaki et al., 1996).

Tight coordination between the development of the *C. elegans* somatic gonad and germ line is essential for germline patterning and function. Normal germline development and maintenance of the stem cell pool as well as regulation of oocyte growth requires distal tip cell (DTC) production of the DSL family ligands LAG-2 and APX-1 (Henderson et al., 1997; Nadarajan et al., 2009). Previously, we found that a latent proliferation-promoting

signal from the proximal gonad lineage can promote the formation of proximal germline tumors (Pro phenotype) in certain mutant backgrounds (Killian and Hubbard, 2005; McGovern et al., 2009). This hypothesis was supported by the observations that (1) the Pro phenotype is suppressed by removal of a subset of the proximal somatic gonad lineage by laser microsurgery or by downregulation of *apx-1, arg-1* or *dsl-5*, (2) transcriptional reporters for the DSL ligands, *apx-1* and *arg-1* are expressed in the proximal somatic gonadal lineage (3) depletion of *apx-1* by RNAi in individuals that already formed a tumor permits differentiation of the tumor (McGovern et al., 2009). All told, the data support a model in which these DSL ligands promote the maintenance and growth of tumors that form when DSL ligand-expressing cells of the proximal somatic gonad are inappropriately juxtaposed to mitotic germ cells, as occurs in certain mutants.

The “latent niche” activity of these DSL ligand-expressing proximal somatic gonadal cells promotes germline tumor formation. However, this activity is the result of an abnormal anatomical juxtaposition of GLP-1/Notch expressing germ cells with the proximal somatic gonad. We therefore wondered what might be the normal role for APX-1-driven Notch signaling in the proximal somatic gonad. Guided by our previous observation of *apx-1* reporter expression in the proximal somatic gonadal sheath and the distal spermatheca (McGovern et al., 2009), we examined the consequences of reducing *apx-1* activity on oogenesis. Here we define a somatic role for APX-1 in adulthood for normal ovulation.

MATERIALS AND METHODS

Worm methods

Standard methods were used for worm husbandry and genetics (Brenner, 1974). Temperature shift experiments were carried out from stocks raised on OP50.

Strains and plasmids

Strains used (all obtained from the *C. elegans* stock center (CGC) unless otherwise referenced): N2 Bristol wild type, PD8488 *rrf-1*(*pk1417*) (Sijen et al., 2001), *apx-1*(*or3*) isolated from GC759 *apx-1(or3)/nT1[qIs51]*, GC1139 *naIs39 [pGC506 (Plim-7::PHdomain::mCherry::unc-54 3′UTR-unc-119(+))]; zuIs45 [Pnmy-2::NMY-2::GFP-unc-119(+)]* (Voutev et al., 2009), VP24 *let-502::GFP* (gift from Kevin Strange), CB4108 *fog-2*(*q71*), PS3653 *ipp-5*(*sy605*), GC952 *naEx152* (McGovern et al., 2009), NL2099 *rrf-3(pk1426)*, UN1108 *xbIs1101[Pfln-1::GCaMP]* (Kovacevic et al., 2013), GS60 *unc-32(e189) lin-12(n676n930)* (Sundaram and Greenwald, 1993), CB189 *unc-32*, GC832 *glp-1(e2141)* (Priess et al., 1987).

RNAi

Strains were maintained at 20°C on NGM plates supplemented with 1 mg/ml IPTG and 100 μg/ml ampicillin seeded with the *E. coli* strain HT115 carrying the empty RNAi vector L4440 prior to experiment. RNAi was initiated at different times for different experiments as follows.

Embryo RNAi – (used in trapping assay, see below): embryos from UN1108 (GCaMP expressing) adult gravid worms were collected using an alkaline hypochlorite solution as described in (Hope, 1999) and washed three times in M9 buffer (22 mM KH_2PO_4, 42 mM $NaHPO_4$, 86mM NaCl, and 1mM $MgSO_4$) ('egg prep'). Clean embryos were transferred to supplemented NGM plates seeded with HT115(DE3) bacteria expressing dsRNA of interest and left to incubate at 23°C for 50 hours

L1 experiments: L1 animals were synchronized by "hatch-off" (Pepper et al., 2003), placed on either control, *apx-1* [pGC304; (Nadarajan et al., 2009)], *lin-12*, or *glp-1* RNAi-inducing bacteria (Kamath et al., 2003), then shifted to 25°C for 2–3 days.

L4 experiments: L4 worms were selected and placed on control or RNAi-inducing bacteria, shifted to 25°C, for 1–2 days.

Adult RNAi: Several methods were used. For Table 1, lines 15–18: L1 animals were synchronized by "hatch-off" (Pepper et al., 2003), and grown on L4440-containing bacteria and young adults were selected onto either control or RNAi-inducing bacteria and shifted to 25°C, then scored 1 day later. For Table 1, lines 19–24: L4 animals were selected from OP50 bacteria, grown on L4440-containing bacteria, and young adults were selected onto either control or RNAi-inducing bacteria, shifted to 25°C, then scored 1 or 2 days later. For spermatheca morphology and occupancy analysis, animals were fed OP50, and transferred to RNAi bacteria as young adults at 25°C and scored 24 hr later.

Adult Temperature shift

Each strain was grown and shifted with its respective control. For *lin-12*, GS60 and CB189 were maintained at 20°C, and subsequently shifted to 25°C as early adults. Animals were scored 4–5 and 24 hours later. For *glp-1*, GC832 and N2 were maintained at 15°C and shifted and scored as above.

Emo analysis

Enlarged nuclei characteristic of endomitotic oocytes (Iwasaki et al., 1996) were observed in whole-mount preparations after ~10 minute fixation in EtOH and staining with 4′,6-diamidino-2-phenylindole (DAPI). Gonad arms with one or more endomitotic oocytes in the proximal oviduct (distal to the spermatheca), were scored as Emo. Additionally, large irregular polyploid oocytes were occasionally seen in the uterus. These were scored separately. All animals were scored using a Zeiss Z1 AxioImager with Apotome equipped with an AxioCam monochrome camera and Zeiss Axiovision software.

Measurement of meiotic maturation/ovulation rate

(Modified from (McCarter et al., 1999)). Meiotic maturation and ovulation are coupled in *C. elegans* with meiotic maturation being the rate-limiting step. Female L1 *fog-2(q71)* larvae were synchronized by "hatch off" (Pepper et al., 2003) and raised at 25°C on either control (L4440) or *apx-1* RNAi. Individual young adults were placed in a drop of M9 on an agar pad and viewed using Nomarski microscopy. The total number of eggs (unfertilized oocytes and/or embryos depending on mating) retained in the uterus was determined (T1). Animals

were transferred to individual plates containing the same RNAi treatment they were originally fed and allowed to lay eggs at 25°C for ~5 hours (the exact time was recorded). The number of eggs laid on each plate plus the number of eggs retained in the uterus was then determined (T2). The rate of egg production was determined by subtracting the number of eggs retained at T1 from the number of eggs laid plus retained at T2, and calculating the rate per gonad arm in one hour as (number retained + number laid at T2) – (number retained at T1)/time interval = egg production rate per hour. Rate per hour was then divided by 2 (for 2 gonad arms) to arrive at rate per gonad arm per hour.

Mating experiment

(Modified from (McGovern et al., 2007)). Female L4 *fog-2(q71)* larvae that were synchronized using the L1 hatch off method and raised at 25°C on either control (L4440) or *apx-1* RNAi were selected and allowed to mature at 25°C overnight on the same RNAi treatment they were raised on. Approximately 15 wild-type (N2) male worms, grown at 25°C on L4440 were selected and placed on a plate with ~3 young adult *fog-2* females and allowed to mate for a minimum of 2 hours. The maturation rate per gonad arm per hour was calculated (see above) only in animals that had mated (contained sperm). Parallel mated and unmated animals were DAPI stained to score for the Emo phenotype.

Trapping assay

Embryos from UN1108 (GCaMP expressing) embryos were exposed to RNAi inducing bacteria as described above. Upon reaching adulthood, nematodes were killed in a drop of 0.08 M sodium azide and mounted on 2% agarose pads to be visualized using a 60x oil-immersion objective with a Nikon Eclipse 80i epifluorescence microscope equipped with a Spot RT3 CCD camera (Diagnostic instruments; Sterling Heights, MI, USA). Animals were scored for the presence or absence of an embryo in the spermatheca as well as entry defects such presence of small fragments of oocytes and an open distal neck. A Fisher exact *t*-test (two dimensional x^2 analysis) using GraphPad Prism statistical software was used to compare between RNAi treatments the percent of occupied spermathecae.

Acquisition of DIC and GCaMP time lapse series

Slides were prepared by placing animals in 10 μl M9 buffer and 5 μl Polystyrene 0.05 Micron Microspheres beads on 5% agarose pads and imaged using a 60× oil immersion objective with a Nikon Eclipse 80i microscope equipped for wide-field epifluorescence and differential interference contrast (DIC). The approximate transverse cross-section of the spermatheca was selected as the focal plane. Fluorescence excitation was provided by a Nikon Intensilight C-HGFI 130W mercury lamp. Neutral density filters were used to reduce illumination intensity to 3.1% (1/32). Fluorescence excitation light was shuttered with a SmartShutter (Sutter Instruments; Novato, CA, USA), and controlled via the camera TTL signal. A SPOT RT3 cooled charge-coupled device camera (Diagnostic Instruments; Sterling Heights, MI, USA) was used to capture images at 1 frame per second using SPOT Advanced 5 (Diagnostic Instruments). For GCaMP imaging, the camera exposure time, gain, and binning were set to 75 ms, 8, and 1×1, respectively. All light was redirected to the camera, and the DIC analyzer was removed from the light path. The same microscopy setup was used for all experiments. Room temperature was maintained between 20 and 23°C.

Image Processing for time-lapse experiments

Images were acquired at 1600×1200 pixels and saved as 8-bit tagged image file format (TIFF) files. All image processing was done using ImageJ (National Institutes of Health; Bethesda, MD, USA; http://rsb.info.nih.gov/ij/). The GCaMP signal was measured by defining a region of interest around the spermatheca with a standard size of 800×400 pixels (100 μm × 50 μm). The mean pixel intensity (total pixel intensity/area) for each frame was then calculated using a custom ImageJ macro. We expressed the GCaMP signal (F) as a ratio with the baseline fluorescence (F0). The baseline fluorescence was calculated as the mean fluorescence of 30 frames preceding the ovulation. Data analysis and plotting were performed with GraphPad Prism 5. Kymograms were generated using a custom ImageJ macro to determine the mean fluorescence intensity of each column of pixels and represent it as a single pixel in the kymogram. Movies were exported as Audio Video Interleave (AVI) files from ImageJ and subsequently encoded as QuickTime (Apple; Cupertino, CA, USA) H. 264 movies and scaled down to 400×200 pixels. The normalized pixel intensity traces were converted to heat maps using a custom ImageJ macro.

RESULTS and DISCUSSION

Reduction of *apx-1* activity causes a soma-dependent Emo phenotype

In previous work investigating the cellular mechanism of proximal germline tumor formation, we found that *apx-1* is expressed in the proximal somatic gonad lineage, specifically in the proximal sheath and distal spermatheca (McGovern et al., 2009). *apx-1* contributes to proximal tumor formation under abnormal situations in which germ cells expressing the GLP-1/Notch receptor are inappropriately juxtaposed to APX-1 expressing proximal sheath cells. We therefore wondered whether *apx-1* had a role in normal gonad development. Given the expression pattern of the *apx-1* reporter, we examined oocytes in the proximal oviduct.

We observed an endomitotic oocyte (Emo) phenotype in animals with reduced *apx-1* activity. Both *apx-1(or3)* mutants and animals treated as L1 larvae with *apx-1* RNAi displayed an Emo phenotype with incomplete penetrance (14% and 20% respectively) (Table 1; Figure 1A, B). Two other *apx-1* mutants, *apx-1(zu183)* and *apx-1(zu212),* did not exhibit an Emo phenotype (data not shown) even though, like *apx-1(or3)*, they exhibited a completely penetrant maternal effect lethal phenotype. Taken together with results from our previous observations (McGovern et al., 2009), these results suggest that *apx-1(zu183)* and *apx-1(zu212)* are weaker or that they do not share the same tissue-specific effects as *apx-1(or3)*.

Because soma-germline communication is important for proper oocyte maturation and ovulation, endomitotic oocytes can form as a result of defects in the germ line or the soma (Kim et al., 2013). To assess the soma versus germline autonomy of the *apx-1*RNAi Emo phenotype, we used the *rrf-1(pk1417)* strain in which RNAi is compromised in somatic tissues but is effective in the germ line (Kumsta and Hansen, 2012; Sijen et al., 2001). While 20% of *rrf-1(+)* animals treated with *apx-1*RNAi displayed the Emo phenotype, *rrf-1* mutant animals treated with *apx-1* RNAi did not display the Emo phenotype (Table 1). These data

suggest that *apx-1* activity is required in the soma to prevent the formation of endomitotic oocytes. This result is consistent with the expression pattern we observe for *apx-1* in the proximal sheath and distal spermatheca (McGovern et al., 2009).

Reduced *apx-1* activity alters ovulation

Endomitotic oocytes can result from inappropriate meiotic maturation and/or defective ovulation, (Iwasaki et al., 1996). Meiotic maturation occurs at a very low rate in the absence of signals from the sperm. As a proxy for both meiotic maturation and ovulation, we assessed the rate of oocyte production (McCarter et al., 1999) in control and *apx-1* RNAi conditions in unmated “females”, that is, spermless *fog-2(q71)* animals. We found that in both control and *apx-1* RNAi-treated *fog-2* females, oocyte production occurred at a normal low level (Table 2). We then examined mated control or *apx-1* RNAi-treated *fog-2* females. Both displayed an elevation in the rate of egg production per gonad arm per hour relative to the unmated condition (Table 2).

Next, we asked whether the Emo phenotype required the presence of sperm. We compared the frequency with which gonad arms contained endomitotic oocytes in mated and unmated *fog-2(q71*) animals treated with *apx-1* RNAi. In the absence of sperm we did not observe the Emo phenotype. However, in the presence of sperm, 33% of gonad arms displayed the Emo phenotype in *apx-1* RNAi animals (Table 1). We did not observe any endomitotic oocytes in the gonads of either mated or unmated females treated with the empty vector, L4440 (Table 1).

Since reducing *apx-1* activity did not cause inappropriate meiotic maturation/ovulation in the absence of sperm, and since the Emo phenotype required the presence of sperm, we hypothesized that defective ovulation might underlie the Emo phenotype. Endomitotic oocytes can accumulate in the oviduct when oocytes have undergone meiotic maturation but are not ovulated (Cecchetelli et al., 2016; Iwasaki et al., 1996). Proper ovulation requires a series of well-orchestrated signaling events involving the somatic gonad sheath, the oocyte, a sperm-produced signal (major sperm protein, MSP), and the distal spermatheca (McCarter et al., 1999; Miller et al., 2001). MSPs produced by mature sperm signal to the sheath to stimulate sheath contractions that are required for ovulation. The oocyte then signals the spermatheca to initiate spermathecal dilation that together with sheath contractions force the oocyte into the spermatheca where sperm reside and fertilization takes place (Clandinin et al., 1998).

To determine whether *apx-1* affected ovulation, we visualized ovulation in live animals using time-lapse microscopy. Normally, the oocyte is ovulated into the spermatheca, transits the spermatheca, and then enters the uterus by way of the spermathecal-uterine (sp-ut) valve (still images in Figure 1C; Supplementary Video 1). In contrast, in *apx-1* depleted animals (embryo or L1 RNAi; see Materials and Methods), oocytes occasionally enter the spermatheca and then slip back into the oviduct following a failure of distal neck closure (still images in Figure 1D; Supplementary Video 2). We analyzed video recordings of ovulation in *apx-1* RNAi depleted animals and compared them with the control animals using the empty RNAi vector L4440. We observed a variety of defects in both the timing and execution of ovulation when *apx-1* activity was reduced. These defects included ovulation

delays after nuclear envelope breakdown, engulfment of a second oocyte before completing the previous ovulation, as well as ovulations in which the oocytes were pinched, torn, or distorted by the spermatheca. We also observed fragments of oocytes in the uterus or oviduct by DIC microscopy as well as grossly polyploid oocytes in the uterus after fixation and staining with DAPI (see Figure 1). Large, irregularly shaped polyploid oocytes in the uterus may have undergone endoreduplication in the oviduct prior to being ovulated. Alternatively they may have become polyploid in the uterus as a result of fragmentation that occurred pre- or post-fertilization. Thus, we speculated that the Emo phenotype was secondary to ovulation failure such that once normal ovulation failed, oocytes that matured in response to MSP – but that could not be ovulated due to blockage from a previous abnormal ovulation – underwent endomitotic divisions in the oviduct.

To further investigate whether *apx-1* plays a role in oocyte entry or transit through the spermatheca, we surveyed populations of young adult animals (~50 hours past hatching) for spermathecal occupancy. In animals with entry defects, few spermathecae contain oocytes, whereas in animals with defects in oocyte transit, oocytes become stuck in the spermatheca and the percentage of occupancy increases. In positive control *plc-1* RNAi treated animals (Kovacevic et al., 2013), 100% (n=103) of spermathecae were occupied by an oocyte. In young adult *apx-1* RNAi animals,15% (n=121) of spermathecae contained oocytes, similar to the control 13% (n=98). Unlike the control, however, fragments of oocytes were observed in 10% (n=121) of spermathecae in animals treated with *apx-1* RNAi (Table 3). In 6 of the 12 spermathecae containing oocyte fragments, the distal neck of the spermatheca was open and oocyte fragments were observed in the oviduct as well. Importantly, none (n=98) of the negative control spermathecae contained oocyte fragments ($p<0.001$, for control versus *apx-1* RNAi by Fisher exact test). These results suggest that the failure of the spermathecal neck to close in a timely manner is an important aspect of the abnormal ovulation and the Emo phenotype seen when *apx-1* activity is reduced.

Spermatheca calcium flux is altered by depletion of *apx-1*

Imaging animals expressing the genetically encoded sensor GCaMP3 enables analysis of calcium transients during ovulation and transit. In animals treated with L4440 control RNAi, a strong calcium pulse in the sp-ut valve is followed by waves of calcium that sweep across the tissue, culminating in contraction of the spermathecal cells and expulsion of the fertilized embryo into the uterus (still images in Figure 2C; Supplementary Video 3). In *apx-1* RNAi animals exhibiting ovulation defects, the calcium signal is also abnormal. The initial pulse in the sp-ut valve is observed, as are oscillations of calcium signal across the tissue. However, when the distal neck fails to close, the strong pulses, which would normally expel the egg into the uterus fail to occur (still images in Figure 2A; Supplementary Video 4). We visualized the entire time series by summing the pixel brightness in each column of each image to a single row, and then stacking the rows to produce kymograms (Figure 2B). The bright signal at the bottom right of each kymogram is the sp-ut valve, and the streaks across the kymogram are the transients that sweep across the tissue. In the vector control animals, the embryo exits following a series of strong calcium pulses (T=410 sec). In contrast, even though calcium flux occurs in affected *apx-1*-depleted animals, the oocyte remains trapped in the spermatheca (>770 sec). It remains unclear whether spermathecal

cells fail to contract due to abnormal calcium flux and this is what causes the neck to remain open, or vice versa. In addition, *apx-1* is expressed in the proximal sheath cells (McGovern et al., 2009) where it could be required for coordination between the sheath and spermatheca that is necessary for proper ovulation.

Reduced *ipp-5* activity partially suppresses defects induced by *apx-1* RNAi

Because *apx-1* is expressed in the distal-most four spermathecal cells as well as in the proximal sheath (Nadarajan et al., 2009), we considered the possibility that the defect in ovulation could result from defects in the spermathecal response to oocyte signaling. Oocyte signaling via LIN-3 activates the LET-23/EGF receptor in the spermatheca and an IP_3 cascade triggers spermathecal dilation (Clandinin et al., 1998). Reduced activity of *ipp-5*, which encodes an IP_3 phosphatase, causes hyper-stimulation of the spermatheca, likely due to an increase in IP_3 levels and subsequent calcium release. A reduction of *ipp-5* activity suppresses ovulation defects and the Emo phenotype caused by reduced *lin-3* or *let-23* (Bui and Sternberg, 2002). To investigate whether elevated IP_3 might similarly suppress the *apx-1* RNAi-induced ovulation defects, we reduced *apx-1* activity by RNAi in *ipp-5*(*sy605*) mutants and found that *ipp-5*(*sy605*) partially suppresses the *apx-1* Emo phenotype. In *ipp-5*(*+*) individuals treated with *apx-1* RNAi, 28% of gonad arms contained endomitotic oocytes, while in similarly treated *ipp-5* mutants, only 8% of gonad arms contained endomitotic oocytes (Table 1). This result is consistent with the possibility that elevated spermathecal calcium release may partially compensate for failure of the neck to close when *apx-1* activity is reduced.

LAG-2 can substitute for APX-1 in ovulation

We tested whether the specific identity of the DSL family ligand was important for this role of APX-1 in ovulation and found that it is not. Previously it has been shown that APX-1 can substitute for LAG-2 in the distal tip cell (Fitzgerald and Greenwald, 1995) and that LAG-2 can substitute for APX-1 in its proximal tumor-promoting role (McGovern et al., 2009). We compared the penetrance of the Emo phenotype of *apx-1* RNAi animals among siblings that either did or did not bear an extrachromosomal array (*naEx152)* expressing P*apx-1::lag-2* (pGC398; (McGovern et al., 2009)). We found that animals carrying the array did not develop endomitotic oocytes whereas those without the array did (Table 1). We conclude that LAG-2 can substitute for APX-1 in its role in ovulation.

APX-1 likely acts with LIN-12

We next asked which of the two Notch receptors in *C. elegans* might mediate these effects of APX-1. Because mutations in either *glp-1* or *lin-12* cause severe and confounding developmental defects in the germ line (Austin and Kimble, 1987) and somatic gonad (Greenwald et al., 1983), respectively, we restricted RNAi to adulthood. For *glp-1*, we did not see statistically significant elevation in the Emo phenotype (Table 1). However, since loss of *glp-1* causes depletion of the distal stem cell pool (Austin and Kimble, 1987) and abnormal growth of oocytes (Nadarajan et al., 2009), it is difficult to cleanly assess a role in ovulation, even when its depletion is restricted to adulthood. In contrast, in these experiments *lin-12* RNAi caused a significant penetrance of the Emo phenotype, similar to that observed with *apx-1* RNAi (Table 1; see also below).

Sheath and spermatheca markers persist in individual *apx-1* and *lin-12* RNAi-treated animals that display ovulation defects

The Notch signaling pathway is best known for its role in cell fate specification, yet our adult RNAi results suggested that the Emo phenotype may be due to an adult defect, independent of previous cell fate specification during development. To assess the state of cell fate specification in the sheath and spermatheca vis-à-vis ovulation defects, we examined a *lim-7::mCherry* reporter that is expressed in all 5 pairs of sheath cells (Voutev et al., 2009) in both control and *apx-1* RNAi, treated from the L1 stage. Expression of the reporter in sheath cells was normal in 100% of the gonadal arms examined, in both control and *apx-1* RNAi animals (Table 4). We noted that expression was directly observed in the gonad arms that contained pieces of oocytes in the oviduct, spermatheca or the distal uterus as a result of *apx-1* RNAi (Figure 3A; Table 4). Next we examined *lim-7::mCherry* expression in both control and *lin*-12 RNAi-treated animals (treated from the L1 stage) and observed expression of the reporter in 100% of control and *lin-12* RNAi animals (Table 4), even in the gonads that contained pieces of oocytes in the oviduct, spermatheca or uterus (Figure 3B; Table 4). Thus, based on this marker, the overall integrity or identity of the sheath does not appear to be compromised in animals that display ovulation defects.

Next, we examined expression of *let-502::GFP* in the distal spermathecal cells, after feeding control and *apx-1* RNAi starting in the L1. We found that expression of the reporter was unaltered in 100% of both control and the *apx-1* RNAi-treated animals (Table 4). Similar to what we had observed with the sheath marker, *let-502::GFP* expression was normal even in the 21% gonadal arms that contained pieces of oocytes (Figure 3C; Table 4). Similarly, when we examined the *let-502::GFP* reporter in both control and *lin*-12 RNAi-treated animals, we again observed expression of the marker in 100% of control and *lin-12* RNAi-treated animals, even in the gonads that contained pieces of oocytes; (Figure 3D; Table 4). Similar to our analysis of the sheath, based on this marker, our data suggest that the overall identity of the spermathecal cells is not compromised even in animals that display ovulation defects.

APX-1 and LIN-12 may act in adulthood

To explore further a role for *lin-12* and to determine whether *apx-1* and *lin-12* might be required post-developmentally, we treated young adult wild-type worms with RNAi and scored Emo and spermathecal morphology. As noted above, in the set of experiments performed in parallel with the adult *glp-1 RNAi*, we found that both *apx-1* and *lin-12* showed a statistically significant penetrance of the Emo phenotype compared to those treated with the empty vector L4440, whereas animals fed *glp-1* RNAi-inducing bacteria did not (Table 1). In these experiments, animals were raised from hatching on HT115 bacteria bearing the empty vector and then switched to the test RNAi as young adults, and scored a day later. In a separate set of experiments, however, the penetrance of the phenotype was markedly reduced (0% for all at 24 hr, and 11% for *apx-1* and 0% for *lin-12* after 48 hr; Table 1). In this case, animals were raised initially on OP50 bacteria until the L4 stage, when they were put on HT115 with the control L4440, and then as young adults were moved to test (or control) RNAi bacteria for 24 or 48 hr. Therefore, the phenotypes are highly sensitive to RNAi conditions.

We then turned to the *rrf-3* mutant background (Simmer et al., 2003; Simmer et al., 2002) to see if it would enhance the effect of RNAi as we had seen previously with *lin-12* (Pekar et al., 2017). In this background, we observed a low penetrance of the Emo phenotype after 24 hr RNAi in the *lin-12* RNAi condition (6%, n=54, not significant by 1-sided Fisher exact test), and 0% of the gonads displaying the Emo phenotype in the control (n=53). In an independent set of experiments, we scored for the open spermathecal neck defect after 24 hours of RNAi feeding starting at the young adult stage. In these conditions, 0% of the *rrf-3* mutants fed RNAi control displayed an open spermathecal neck (n=82), while the spermatheca in 15% of *apx-1* RNAi (n=89) and 21% of *lin-12* RNAi (n=72) had an open neck (Table 3). These animals also had pieces of oocytes in the oviduct, suggesting that defective ovulation had occurred. Therefore, although the penetrance of these RNAi defects is low and is variable, given that the phenotype may be somewhat cumulative and that RNAi typically has a low rate of false positives, our results suggest that an APX-1/LIN-12 dependent signaling pathway may act during adulthood to maintain proper ovulation.

To further assess post-developmental effects of reduced *lin-12* on ovulation, we took advantage of a temperature-sensitive allele, *lin-12(n676n930),* that displays partial loss-of-function character at the restrictive temperature of 25°C (Sundaram and Greenwald, 1993). We did not observe Emo or irregularly shaped polyploid oocytes in the uterus of control *unc-32(e189)* or *lin-12* mutant gonad arms scored at 5 hours post-shift (n=60 and 91, respectively). However, after 24 hours at the restrictive temperature 4% of *lin-12* gonad arms contained endomitotic oocytes while 16% contained irregularly shaped highly polyploid oocytes in the uterus (n=50; p not significant for Emo and $p < 0.001$ for abnormal oocytes, 1-sided Fisher exact test). The control animals (n=70) displayed neither phenotype. In independent experiments assessing spermathecal morphology and contents, however, we did not observe defects when animals were scored after 4 or 24 hours at the restrictive temperature. That is, there was no significant difference in the penetrance of the open neck or of oocyte pieces in the gonad between *unc-32(e189)* or *lin-12* mutant gonad arms (n=285 and 150, respectively at the 4 hour time point and n=123 and 104 respectively at the 24 hour time point). For the temperature-shift Emo assessment experiment and for the 4 hour time point for spermathecal morphology, *glp-1(e2141)* and control (N2) worms shifted from 15°C to 25°C were assessed in parallel. In no case were significant differences observed in comparison with the control. In sum, the combined results of the RNAi and genetic experiments suggest that post-developmental effects of reduced *apx-1* and *lin-12* activity may contribute to defects in ovulation.

How might APX-1 signaling influence ovulation during adulthood?

Although no gross defects in sheath and spermathecal markers were noted (Figure 3), and there is a modest effect of reducing the pathway activity in adulthood, it remains possible that a subtle developmental defect would not become apparent until the sheath and spermatheca were challenged with oocyte entry that may, in addition to adult effects, contribute to the phenotype. Consistent with this idea, we occasionally observed abnormally weak or slightly disorganized phalloidin staining of F-actin in the proximal sheath (data not shown). However this phenotype did not correlate with the Emo phenotype in individual gonad arms.

Additionally, APX-1 is also expressed in the DTC where it influences the size of the germline progenitor pool and, at low penetrance, the size of oocytes (Nadarajan et al., 2009). The latter phenotype may be relevant since it may be more difficult for the spermatheca to remain closed over a larger oocyte. However, we do not favor this explanation since we did not see an obvious change in oocyte size in our experiments, nor did we see similar phenotypes with *glp-1*.

Defects in ovulation resulting from adult depletion of *apx-1* may originate from failures in maintenance of relevant cell fates, of signaling, and/or in the physical mechanics of ovulation. In the future, it will be important to examine further the cellular focus of activity of *apx-1* and *lin-12*. Additional open questions are how expression and activity of the ligand and receptor are regulated, whether other ligands are involved, whether the morphology and fate of the sheath and spermatheca are maintained in the absence of signaling, and how signaling integrates with the regulation of other specific molecular and physical aspects of ovulation such as the control of sheath contractions and spermathecal dilation. For example, APX-1-dependent effects on ovulation may result from a continuous requirement for signaling that coordinates with cues from the germ line or from other somatic cells to ensure spermathecal closure after the oocyte enters the spermatheca.

Post-mitotic neuronal roles for continuous Notch signaling have been described in many systems, including sleep regulation and synaptic plasticity characterized in *C. elegans*, *Drosophila* and mammals (Alberi et al., 2011; Ge et al., 2004; Presente et al., 2004; Seugnet et al., 2011; Singh et al., 2011). These studies led to the hypothesis that Notch signaling is sensitive to environmental stressors (Wu and Raizen, 2011). Fewer examples have been described for non-proliferative responses in non-neuronal tissue. Recently, Notch1 was found to be up-regulated in response to wounding in mammalian keratinocytes where it alters cell migration (Na et al., 2017). In *C. elegans*, DSL ligand expression in the larval DTC was found to respond to nutrient deprivation via TGFβ-mediated transcriptional regulation, where it impacts the size of the germline stem cell pool (Pekar et al., 2017). It will be of interest to determine whether APX-1-dependent regulation of ovulation is similarly altered by changes in environmental conditions.

Supplementary Material

Refer to Web version on PubMed Central for supplementary material.

Acknowledgments

We thank John Maciejowski who began this line of investigation, and Nance and Hubbard lab members for discussion. This work was supported by the National Institutes of Health R01GM061706 to E.J.A.H., R01GM110268 to E.J.C., and a Kimmel Stem Cell Fellowship to MM. Some strains were provided by the CGC, which is funded by NIH Office of Research Infrastructure Programs (P40 OD010440).

REFFERENCES

Alberi L, Liu S, Wang Y, Badie R, Smith-Hicks C, Wu J, Pierfelice TJ, Abazyan B, Mattson MP, Kuhl D, Pletnikov M, Worley PF, Gaiano N. Activity-induced Notch signaling in neurons requires Arc/Arg3.1 and is essential for synaptic plasticity in hippocampal networks. Neuron. 2011; 69:437–444. [PubMed: 21315255]

Austin J, Kimble J. glp-1 is required in the germ line for regulation of the decision between mitosis and meiosis in C. elegans. Cell. 1987; 51:589–599. [PubMed: 3677168]

Brenner S. The genetics of Caenorhabditis elegans. Genetics. 1974; 77:71–94. [PubMed: 4366476]

Bui YK, Sternberg PW. Caenorhabditis elegans inositol 5-phosphatase homolog negatively regulates inositol 1,4,5-triphosphate signaling in ovulation. Molecular biology of the cell. 2002; 13:1641–1651. [PubMed: 12006659]

Cecchetelli AD, Hugunin J, Tannoury H, Cram EJ. CACN-1 is required in the Caenorhabditis elegans somatic gonad for proper oocyte development. Developmental biology. 2016; 414:58–71. [PubMed: 27046631]

Chao MY, Larkins-Ford J, Tucey TM, Hart AC. lin-12 Notch functions in the adult nervous system of C. elegans. BMC neuroscience. 2005; 6:45. [PubMed: 16011804]

Chen N, Greenwald I. The lateral signal for LIN-12/Notch in C. elegans vulval development comprises redundant secreted and transmembrane DSL proteins. Developmental cell. 2004; 6:183–192. [PubMed: 14960273]

Clandinin TR, DeModena JA, Sternberg PW. Inositol trisphosphate mediates a RAS-independent response to LET-23 receptor tyrosine kinase activation in C. elegans. Cell. 1998; 92:523–533. [PubMed: 9491893]

Fitzgerald K, Greenwald I. Interchangeability of Caenorhabditis elegans DSL proteins and intrinsic signalling activity of their extracellular domains in vivo. Development. 1995; 121:4275–4282. [PubMed: 8575327]

Ge X, Hannan F, Xie Z, Feng C, Tully T, Zhou H, Xie Z, Zhong Y. Notch signaling in Drosophila long-term memory formation. Proceedings of the National Academy of Sciences of the United States of America. 2004; 101:10172–10176. [PubMed: 15220476]

Greenwald, I., Kovall, R. WormBook. The C. elegans Research Community. WormBook; 2013. Notch signaling: genetics and structure. http://www.wormbook.org

Greenwald IS, Sternberg PW, Horvitz HR. The lin-12 locus specifies cell fates in Caenorhabditis elegans. Cell. 1983; 34:435–444. [PubMed: 6616618]

Henderson ST, Gao D, Christensen S, Kimble J. Functional domains of LAG-2, a putative signaling ligand for LIN-12 and GLP-1 receptors in Caenorhabditis elegans. Molecular biology of the cell. 1997; 8:1751–1762. [PubMed: 9307971]

Hope, IA. C. elegans: A Practical Approach. Oxford University Press; 1999.

Iwasaki K, McCarter J, Francis R, Schedl T. emo-1, a Caenorhabditis elegans Sec61p gamma homologue, is required for oocyte development and ovulation. The Journal of cell biology. 1996; 134:699–714. [PubMed: 8707849]

Jarriault S, Schwab Y, Greenwald I. A Caenorhabditis elegans model for epithelial-neuronal transdifferentiation. Proceedings of the National Academy of Sciences. 2008; 105:3790–3795.

Kamath RS, Fraser AG, Dong Y, Poulin G, Durbin R, Gotta M, Kanapin A, Le Bot N, Moreno S, Sohrmann M, Welchman DP, Zipperlen P, Ahringer J. Systematic functional analysis of the Caenorhabditis elegans genome using RNAi. Nature. 2003; 421:231–237. [PubMed: 12529635]

Karp X, Greenwald I. Control of cell-fate plasticity and maintenance of multipotency by DAF-16/FoxO in quiescent Caenorhabditis elegans. Proceedings of the National Academy of Sciences. 2013; 110:2181–2186.

Killian DJ, Hubbard EJA. Caenorhabditis elegans germline patterning requires coordinated development of the somatic gonadal sheath and the germ line. Developmental biology. 2005; 279:322–335. [PubMed: 15733661]

Kim S, Spike C, Greenstein D. Control of oocyte growth and meiotic maturation in Caenorhabditis elegans. Advances in experimental medicine and biology. 2013; 757:277–320. [PubMed: 22872481]

Kovacevic I, Orozco JM, Cram EJ. Filamin and phospholipase C-epsilon are required for calcium signaling in the Caenorhabditis elegans spermatheca. PLoS genetics. 2013; 9:e1003510. [PubMed: 23671426]

Kumsta C, Hansen M. C. elegans rrf-1 Mutations Maintain RNAi Efficiency in the Soma in Addition to the Germline. PLoS ONE. 2012; 7:e35428. [PubMed: 22574120]

Li P, Collins KM, Koelle MR, Shen K. LIN-12/Notch signaling instructs postsynaptic muscle arm development by regulating UNC-40/DCC and MADD-2 in Caenorhabditis elegans. eLife. 2013; 2:73–29.

McCarter J, Bartlett B, Dang T, Schedl T. On the control of oocyte meiotic maturation and ovulation in Caenorhabditis elegans. Developmental biology. 1999; 205:111–128. [PubMed: 9882501]

McGovern M, Voutev R, Maciejowski J, Corsi AK, Hubbard EJA. A "latent niche" mechanism for tumor initiation. Proceedings of the National Academy of Sciences. 2009; 106:11617–11622.

McGovern M, Yu L, Kosinski M, Greenstein D, Savage-Dunn C. A role for sperm in regulation of egg-laying in the nematode C. elegans. BMC developmental biology. 2007; 7:41. [PubMed: 17472754]

Miller MA, Nguyen VQ, Lee MH, Kosinski M, Schedl T, Caprioli RM, Greenstein D. A sperm cytoskeletal protein that signals oocyte meiotic maturation and ovulation. Science. 2001; 291:2144–2147. [PubMed: 11251118]

Na J, Shin JY, Jeong H, Lee JY, Kim BJ, Kim WS, Yune TY, Ju BG. JMJD3 and NF-kappaB-dependent activation of Notch1 gene is required for keratinocyte migration during skin wound healing. Scientific reports. 2017; 7:6494. [PubMed: 28747631]

Nadarajan S, Govindan JA, McGovern M, Hubbard EJA, Greenstein D. MSP and GLP-1/Notch signaling coordinately regulate actomyosin-dependent cytoplasmic streaming and oocyte growth in C. elegans. Development. 2009; 136:2223–2234. [PubMed: 19502484]

Ouellet J, Li S, Roy R. Notch signalling is required for both dauer maintenance and recovery in C. elegans. Development. 2008; 135:2583–2592. [PubMed: 18599512]

Pekar O, Ow MC, Hui KY, Noyes MB, Hall SE, Hubbard EJA. Linking the environment, DAF-7/TGFβ signaling and LAG-2/DSL ligand expression in the germline stem cell niche. Development. 2017; 144:2896–2906. [PubMed: 28811311]

Pepper ASR, Killian DJ, Hubbard EJA. Genetic analysis of Caenorhabditis elegans glp-1 mutants suggests receptor interaction or competition. Genetics. 2003; 163:115–132. [PubMed: 12586701]

Presente A, Boyles RS, Serway CN, de Belle JS, Andres AJ. Notch is required for long-term memory in Drosophila. Proceedings of the National Academy of Sciences of the United States of America. 2004; 101:1764–1768. [PubMed: 14752200]

Priess, JR. WormBook. The *C. elegans* Research Community. WormBook; 2005. Notch signaling in the C. elegans embryo. http://www.wormbook.org

Priess JR, Schnabel H, Schnabel R. The glp-1 locus and cellular interactions in early C. elegans embryos. Cell. 1987; 51:601–611. [PubMed: 3677169]

Rasmussen JP, English K, Tenlen JR, Priess JR. Notch signaling and morphogenesis of single-cell tubes in the C. elegans digestive tract. Developmental cell. 2008; 14:559–569. [PubMed: 18410731]

Seugnet L, Suzuki Y, Merlin G, Gottschalk L, Duntley SP, Shaw PJ. Notch signaling modulates sleep homeostasis and learning after sleep deprivation in Drosophila. Curr Biol. 2011; 21:835–840. [PubMed: 21549599]

Siebel C, Lendahl U. Notch Signaling in Development, Tissue Homeostasis, and Disease. Physiological Reviews. 2017; 97:1235–1294. [PubMed: 28794168]

Sijen T, Fleenor J, Simmer F, Thijssen KL, Parrish S, Timmons L, Plasterk RH, Fire A. On the role of RNA amplification in dsRNA-triggered gene silencing. Cell. 2001; 107:465–476. [PubMed: 11719187]

Simmer F, Moorman C, van der Linden AM, Kuijk E, van den Berghe PV, Kamath RS, Fraser AG, Ahringer J, Plasterk RH. Genome-wide RNAi of C. elegans using the hypersensitive rrf-3 strain reveals novel gene functions. PLoS biology. 2003; 1:E12. [PubMed: 14551910]

Simmer F, Tijsterman M, Parrish S, Koushika SP, Nonet ML, Fire A, Ahringer J, Plasterk RH. Loss of the putative RNA-directed RNA polymerase RRF-3 makes C. elegans hypersensitive to RNAi. Curr Biol. 2002; 12:1317–1319. [PubMed: 12176360]

Singh K, Chao MY, Somers GA, Komatsu H, Corkins ME, Larkins-Ford J, Tucey T, Dionne HM, Walsh MB, Beaumont EK, Hart DP, Lockery SR, Hart AC. C. elegans Notch Signaling Regulates Adult Chemosensory Response and Larval Molting Quiescence. Current biology. 2011; 21:825–834. [PubMed: 21549604]

Sundaram M, Greenwald I. Genetic and phenotypic studies of hypomorphic lin-12 mutants in Caenorhabditis elegans. Genetics. 1993; 135:755–763. [PubMed: 8293977]

Voutev R, Keating R, Hubbard EJA, Vallier LG. Characterization of the Caenorhabditis elegans Islet LIM-homeodomain ortholog, lim-7. FEBS letters. 2009; 583:456–464. [PubMed: 19116151]

Wittenburg N, Eimer S, Lakowski B, Röhrig S, Rudolph C, Baumeister R. Presenilin is required for proper morphology and function of neurons in C. elegans. Nature. 2000; 406:306–309. [PubMed: 10917532]

Wu MN, Raizen DM. Notch signaling: a role in sleep and stress. Curr Biol. 2011; 21:R397–398. [PubMed: 21601800]

Highlights

- The DSL ligand *apx-1* is required for normal ovulation
- Ovulation defects include distal spermathecal neck closure delay after oocyte entry
- Oocyte fragmentation and abnormal calcium signals accompany neck closure defects
- Similar phenotypes are observed upon *apx-1* depletion in adults
- Results support a possible post-developmental role for *apx-1* in ovulation

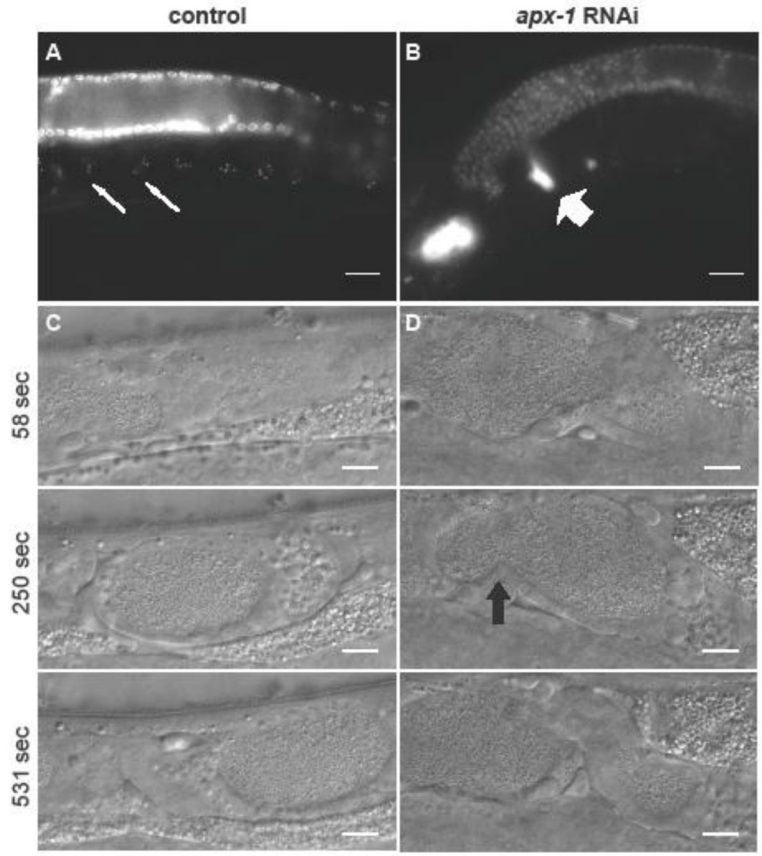

Figure 1. Representative ovulation defects

Examples of normal oocytes in the oviduct of control animal (A) and endomitotic oocyte in the oviduct of animal after *apx-1* RNAi (B) as see in DAPI-stained whole-mount preparations. Small arrows indicate oocyte nuclei; wide arrow (in B) indicates oocyte characteristic of Emo phenotype. Note that the large, irregular DAPI-staining polyploidy oocyte to the left in the uterus is not scored as contributing to the penetrance of Emo (scale bar = 20 μm). Panels C and D are captured from time-lapse microscopy of two individuals that are matched to 58 seconds, 250 seconds, and 531 seconds after oocyte entry. In the control, the oocyte is entering in the first image, is in the spermatheca in the second, and is exiting in the third. Black arrow in second image of individual in D indicates open spermatheca neck (scale bar = 10μm).

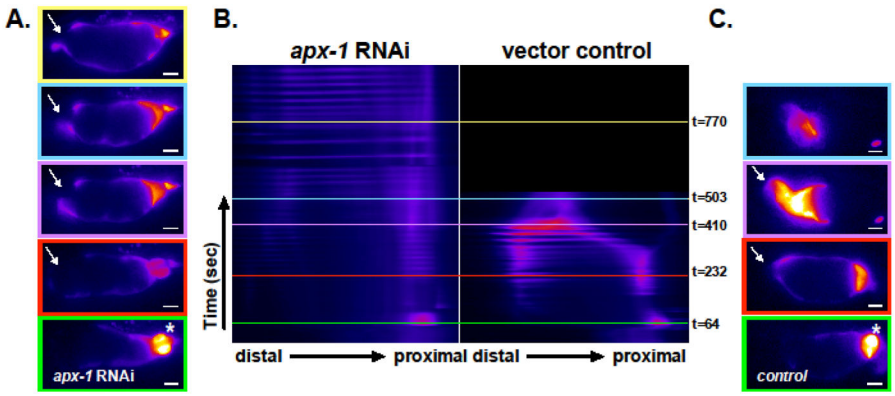

Figure 2. APX-1 is required for distal neck closure and normal calcium signal in the spermatheca

Ovulation events were documented using time lapse microscopy of GCaMP3-expressing animals treated with *apx-1* RNAi or L4440 empty vector control RNAi. Selected frames of an (A) unsuccessful transit observed in an *apx-1* RNAi-treated animal or (C) control wild type transit. Colored boxes indicate the time points for each frame and correspond to the kymograms depicted in (B). The sp-ut valve (proximal) is indicated by an asterisk and the distal neck is indicated by an arrow (scale bars = 10 μm). (B) The kymograms depict calcium signal in each frame, with the data arranged with time (sec) increasing on the y axis and the spatial dimension from distal to proximal on the x axis. The time of wild type entry (t= 64), distal neck closure (t = 232), mid embryo exit (t=410), and complete constriction of the spermatheca after embryo exit (t=503) are indicated by the variously colored lines on the kymogram, corresponding to the colored boxes in (A) and (C). The embryo in the *apx-1* RNAi-treated animal does not exit, as indicated by the occupied spermatheca in A (yellow box) and the broad signal in the *apx-1* RNAi kymogram at t= 770 which indicates the tissue has not contracted.

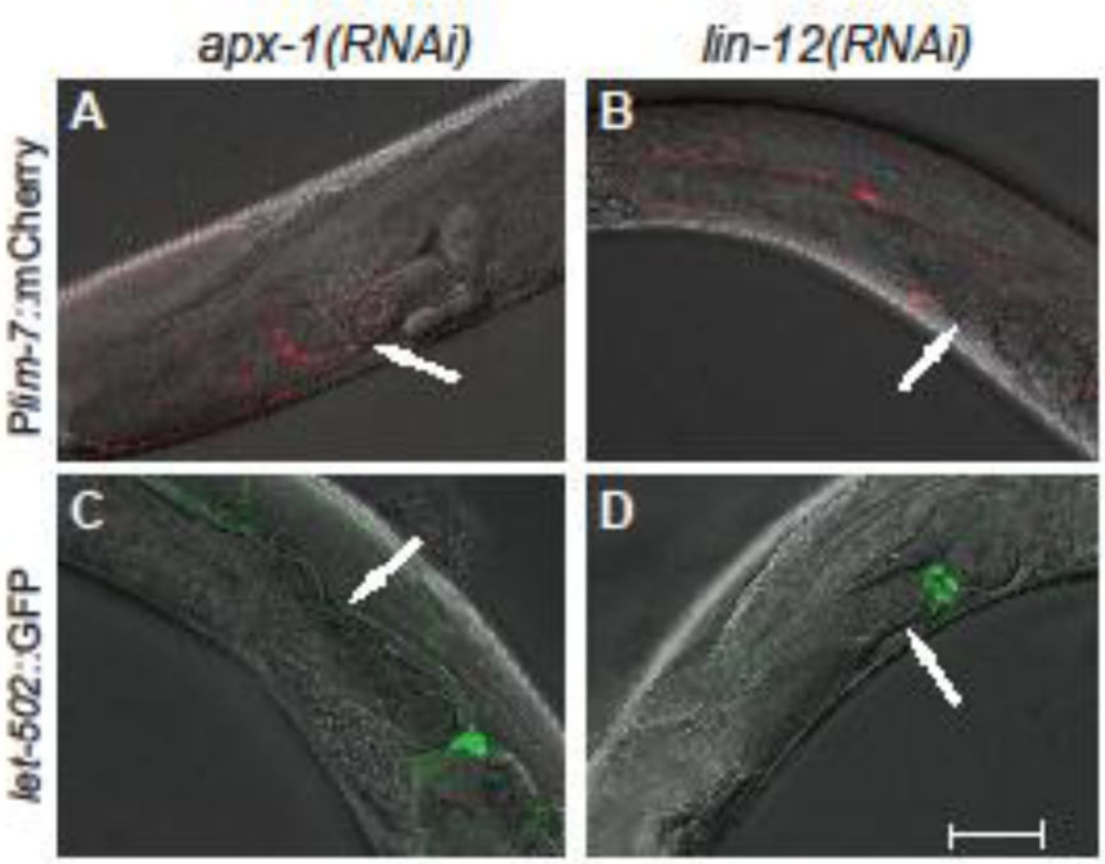

Figure 3. Expression of sheath and spermatheca markers in *apx-1* and *lin-12*-depleted animals with ovulation defects

Individual *apx-1* and *lin-12* RNAi-treated animals expressing P*lim-7::mCherry* (a marker for gonadal sheath cells) and *let-502::GFP* (a marker for the distal spermathecal cells), even when ovulation defects were observed (see Table 3). Arrows indicate abnormal, distorted oocytes (scale bar = 25 μm).

Dev Biol. Author manuscript; available in PMC 2019 March 15.

Table 1

Penetrance of Endomitotic Oocyte (Emo) phenotype

Background	RNAi Treatment[a]	RNAi Method	Percent Emo	n[b]	1-sided Fisher Exact
apx-1(+)	----	---	0%	68	
apx-1(or3)	----	---	14%	88	***
rrf-1(+)[c]	Control[d]	L1	0%	162	
rrf-1(+)[c]	*apx-1*	L1	20%	228	****
rrf-1(−)	Control	L1	0%	127	
rrf-1(−)	*apx-1*	L1	0%	66	
fog-2 Mated	Control	L1	0%	38	
fog-2 Unmated	Control	L1	0%	67	
fog-2 Mated	*apx-1*	L1	33%	72	****
fog-2 Unmated	*apx-1*	L1	0%	40	
ipp-5(+)[c]	Control	L4[e]	0%	171	
ipp-5(+)[c]	*apx-1*	L4	28%	104	
ipp-5(sy605)	Control	L4	0%	167	
ipp-5(sy605)	*apx-1*	L4	8%	53	**
N2	Control	Adult[f]	0%	162	
N2	*apx-1*	Adult	26%	152	****
N2	*lin-12*	Adult	24%	106	****
N2	*glp-1*	Adult	2%	58	ns
N2	Control	Adult[g]	0%	10	
N2	*apx-1*	Adult	11%	18	ns
N2	*lin-12*	Adult	0%	22	ns
rrf-3(−)	Control	Adult[h]	0%	53	
rrf-3(−)	*apx-1*	Adult	0%	48	ns
rrf-3(−)	*lin-12*	Adult	6%	54	ns
$P_{apx\text{-}1::lag\text{-}2}$	Control	L1	0%	51	
Wild type[i]	Control	L1	0%	14	
$P_{apx\text{-}1::lag\text{-}2}$	*apx-1*	L1	0%	12	

Background	RNAi Treatment[a]	RNAi Method	Percent Emo	n[b]	1-sided Fisher Exact
Wild type[i]	*apx-1*	L1	30%	20	*

[a] Due to variability of RNAi, results are separated into experiments that were performed in parallel.

[b] n = number of gonad arms

[c] N2 Wild-type worms.

[d] Control RNAi is the L4440 “empty vector” plasmid in *E. coli* HT115.

[e] The L4 feeding method was used.

[f] Worms were raised on HT115 bacteria from the L1 stage and scored 24 hours after adult shift to control or RNAi-inducing bacteria.

[g] Worms were raised on HT115 bacteria from the L4 stage and scored 48 hours after adult shift to control or RNAi-inducing bacteria.

[h] Worms were raised on HT115 bacteria from the L4 stage and scored 24 hours after adult shift to control or RNAi-inducing bacteria..

[i] Siblings of *P*$_{apx\text{-}1::lag\text{-}2}$ lacking the transgene.

Statistics: 1-sided Fisher exact test, ns= p>0.05, * = p<0.05, **= p <0.01, ***= p<0.001, ****p<0.0001 in pairwise comparison with line above with exception of *fog-2* mated vs unmated, both with *apx-1* RNAi: *ipp-5(+)* and *ipp-5(sy605)*, both with *apx-1* RNAi; N2, all compared pairwise with Control, *P*$_{apx\text{-}1::lag\text{-}2}$ versus wild type, both with *apx-1* RNAi.

Table 2

Depleting *apx-1* activity does not cause inappropriate meiotic maturation and ovulation in the absence of sperm

Background	L1 RNAi	Sperm Present?	Egg production per gonad arm per hour[a]	n[b]
fog-2(*q71*)	Control[c]	No	0.13 ± 0.17	38
fog-2(*q71*)	*apx-1*	No	0.17 ± 0.24	40
fog-2(*q71*)	Control[c]	Yes	2.5 ± 0.93[d]	61
fog-2(*q71*)	*apx-1*	Yes	1.94 ± 1.29[d]	50

[a] "Egg" refers to unfertilized oocytes or embryos depending on mating; rate ± standard deviation.

[b] n = number of gonad arms.

[c] Control RNAi is the L4440 "empty vector" plasmid in *E. coli* HT115.

[d] Not statistically significant (p = 0.07 two-tailed *t*-test)

Table 3

Spermathecal neck closure defects

Background	Condition	Spermathecal neck closure defect (%)	n[a]	1-sided Fisher exact
Wild type[b]	Control[c, d]	0	98	
Wild type	*apx-1*[d]	10	121	***
rrf-3(−)[e]	Control[f]	0	82	
rrf-3(−)[e]	*apx-1*[f]	15	89	***
rrf-3(−)[e]	*lin-12*[f]	21	72	***

[a] n = number of gonad arms

[b] UN1108.

[c] Control RNAi for all is the L4440 “empty vector” plasmid in *E. coli* HT115.

[d] Embryo RNAi method (see Materials and Methods).

[e] NL2099.

[f] Adult RNAi method for spermatheca morphology (see Materials and Methods).

Statistics: 1-sided Fisher exact test, ***= p<0.001, in pairwise comparison with parallel control RNAi in the same strain.

Table 4

Sheath and spermathecal markers are expressed in animals that show evidence of ovulation defects

Marker	L1 RNAi[a]	% Oocyte pieces[b]	% expressing marker	n[c]	1-sided Fisher exact
lim-7::mCherry	Control[d]	0%	100%	42	
lim-7::mCherry	*apx-1*	21%	100%	155	***
lim-7::mCherry	*lin-12*	10%	100%	125	*
let-502::GFP	Control[d]	0%	100%	30	
let-502::GFP	*apx-1*	21%	100%	24	*
let-502::GFP	*lin-12*	13%	100%	30	ns

[a] Due to variability of RNAi, results are separated into parallel control experiments.

[b] Fragments of oocyte in oviduct, spermatheca or uterus as scored with DIC

[c] n = number of gonad arms

[d] Control RNAi is the L4440 “empty vector” plasmid in *E. coli* HT115.

Statistics: 1-sided Fisher exact test, ns= p>0.05, * = p<0.05, ***= p<0.001, in pairwise comparison with control RNAi in the same marker strain.